International Journal of Fluid Power, 2015
Vol. 16, No. 2, 83–98, http://dx.doi.org/10.1080/14399776.2015.1055991

Taylor & Francis
Taylor & Francis Group

An efficient architecture for energy recovery in hydraulic elevators

Oscar R. Peña and Michael J. Leamy*

George W. Woodruff School of Mechanical Engineering, Georgia Institute of Technology, Atlanta, GA 30332-0405, USA

(*Received 23 March 2015; accepted 15 May 2015*)

This study introduces an efficient architecture for hydraulically counter-weighting an elevator system while controlling for cab speed. A physical model of the architecture is developed and posed as a single-input single-output system in which the ratio of two hydraulic pump/motor swash plate angles serve as the control input for regulating the output cab speed. Heuristic control rules based on efficiency considerations and elevator operation are posed for the swash plate angles. A high-fidelity simulation tool is then employed to assess the new architecture and control approach. Simulations demonstrate the effectiveness of the devised control strategy and the overall satisfactory operation of the elevator system. Simulations also provide comparisons of the new architecture's efficiency vs. an electrohydraulic elevator architecture employing a motor/generator for energy capture and return. It's shown that the introduced architecture yields up to a 13% increase in actuation efficiency over the electrohydraulic system, and up to a 23% reduction in input energy over a day's operation. It is anticipated that the gains in energy efficiency, and the reduced complexity and cost (vs. electrohydraulic systems), make the new architecture attractive for continued exploration.

Keywords: hydraulic elevator; energy regeneration; hydraulic transformer; variable-displacement pump/motor

1. Introduction

The practice of converting hydrostatic fluid power into translational or rotational mechanical power is ubiquitous in many industries today. This is typically done through a hydraulic actuator in hydraulic communication with an appropriate hydraulic circuit, and in mechanical communication with its surroundings, such that desired motion is achieved. Common in most forms of power transfer, hydraulic actuation often also has as its goal the movement of a load through a desired motion profile. Supplying enough energy to the hydraulic pump generally fulfills the load requirement. In contrast, contemporary speed or position control varies in technique, efficacy, and efficiency.

Presently, two general approaches achieve motion control of a hydraulic actuator, fluid throttling and displacement control. Motion control via fluid throttling (typically implemented with a load sensing circuit) controls flow into the actuator. Throttling (via flow-control valves) is easily and inexpensively implemented and has a high bandwidth due to the small inertia associated with the throttle valve moving parts. On the other hand, throttling acts by dissipating energy as heat, which renders it highly inefficient (Xu *et al*. 2006, Zimmerman *et al*. 2007, Wang and Li 2012). In contrast, a desired motion profile can also be achieved by controlling the flow output of the pump (displacement control), either via a variable-speed electric motor actuating a fixed-displacement pump, or a variable-displacement pump controlled by a single speed electric drive. Displacement control can entirely eliminate the need for throttling, and therefore the dissipation of energy associated with it, but has a low bandwidth (Oda and Shirai 1997, Mitchell 2001, Grabbel and Ivantysynova 2005, Zimmerman 2008). Additionally, in multiple actuation systems (such as an excavator), a pump for each actuator is needed, resulting in upfront costs much higher than a valve-controlled multi-actuator system; although improvement in overall efficiency can offset costs in the long run (Zimmerman 2008).

The hydraulic elevator has suffered from high inefficiency, a significant part of which stems from a heavy reliance on throttling-based control. This inefficiency largely accounts for its lost market share to traction elevators. In 1986 sales of hydraulic elevators were over 60% higher than those of traction elevators worldwide (Celik and Korbahti 2008a). By 1995, this figure began decreasing due to the introduction of machine room-less (MRL) traction elevators, and has recently reached a market share as low as 40% worldwide while approximately two thirds of new elevators are MRLs since 2010 (Celik and Korbahti 2008b). Additionally, traction elevators boast the benefit of an easily implemented counterweight, further improving their efficiency. Even on mechanically counterweighted hydraulic elevators, the use of throttling valves while descending and stopping dissipates significant energy and negatively impacts the hydraulic elevator's efficiency. Nevertheless, fluid power has advantages over mechanical power transfer, such as high power density, that warrant efforts aimed at improving hydraulic elevator efficiency, especially in low-speed, high pressure applications (Manring *et al*. 2013, Xia and Durfee 2013).

*Corresponding author. Email: michael.leamy@me.gatech.edu

2. Related work

Investigation into the improvement of hydraulic elevators remains active and ongoing since their inception in n.d. by Otis Brothers Co. (Verma), although research on improving efficiency has been a more recent endeavor. In his attempt at an early efficiency improvement, Edwards introduced the concept of a hydraulic counterweight by suggesting the use of a pressurized oil source to capture energy from the cab on its way down (Edwards 1992). Ran studied such a system by incorporating an accumulator as the main oil source in a valve-controlled hydraulic elevator, as shown in Figure 1(a) (Ran 1998). In these systems, the accumulator reduces the pressure differential across the pump, thereby reducing the energy input needed from the electric motor. Descent and ascent of the cab is still regulated via a throttling valve that diverts extra flow during upward motion and restricts flow during downward motion, as needed, to meet a motion profile. The system also has an auxiliary pump system to compensate for leakage over time.

In 1992, researchers from Mitsubishi Electric introduced the first displacement-controlled hydraulic elevator using a variable-speed motor (Shimoaki 1992). Researchers from Bucher Hydraulics also used displacement control and a hydraulic counterweight in communication with the cab via a hydraulic transformer to significantly reduce throttling (Figure 1(b)). Xu further expanded on the concept with several investigations on its movement and efficiency (Xu 2001, Xu *et al*. 2003, Zürcher and Moser 2003, Xu *et al*. 2006). In these architectures, the main speed control component, an electric motor, regulates the torque to the PM in hydraulic communication with the cab. The accumulator supplements the torque provided by the electric motor via its PM during upward motion and reduces the amount of braking torque required during descent. This system almost entirely eliminates the need for a throttling valve and its associated inefficiencies.

Researchers from Bucher Hydraulics further improved this idea by eliminating the hydraulic transformer and using an accumulator again as the primary oil source. Yang studied this idea in detail and provided some insights into its relative efficiency (Moser 2005, Yang *et al*. 2007). In such a design (Figure 1(c)), the main speed control component, again an electric motor/generator, provides and absorbs torque from the system as needed. A highly efficient electrohydraulic design was achieved through the use of an electric generator to recapture some of the energy dissipated by the braking torque. The merits of the electrohydraulic design will be compared and contrasted with the hydraulic design introduced herein. A detailed schematic of the system is reproduced from Yang's work in Figure A1.

3. Hydraulic design

Although not conceived as such, the hydraulic architecture introduced herein can be arrived at through a modification of the design introduced by Bucher Hydraulics, Figure 1(c). By eliminating the electric motor and replacing it with a hydraulic transformer connected to two accumulators, as shown in Figure 2, an architecture results which eliminates the mechanical to electrical energy conversion, and all the associated peripherals

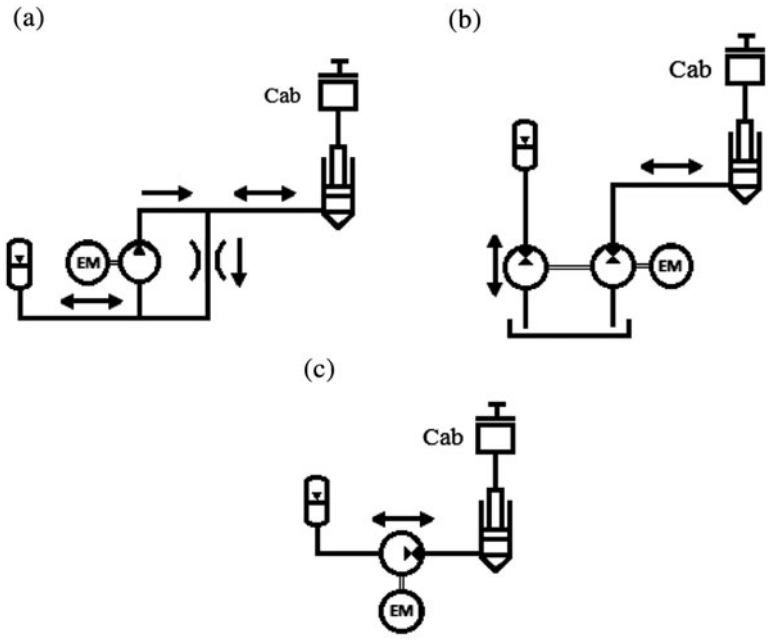

Figure 1. Examples of relevant hydraulic elevator architectures in the literature: (a) valve-controlled, hydraulically counterweighted elevator, (b) elevator hydraulically counterweighted via a hydraulic transformer, (c) hydraulically counterweighted elevator with regenerative braking via an electric generator.

(connection to utilities, battery, converter, etc.) present in the Bucher Hydraulics system. The drawback of the accumulator being characterized by much lower energy density than a battery is of little consequence in stationary applications, such as the elevator (Ven 2009). There are seven primary components in the proposed dual pump/motor speed-controlling hydraulic architecture: two variable-displacement pump/motors, two accumulators, a small auxiliary electric motor (*not* a motor/generator), an actuator, and a reservoir or low-pressure auxiliary accumulator. The main accumulator (Accumulator 1) serves as the main source of fluid for actuation. This connects to the actuator via a main pump/motor (PM_1) that shuttles fluid between the actuator and Accumulator 1. A second pump/motor (PM_2) connects to PM_1 through a shaft and shuttles fluid from a reservoir or low pressure accumulator (Accumulator 3) to a secondary accumulator (Accumulator 2). A small electric machine (EM) serves as a supplemental power source which operates either PM_1 or PM_2 to restore lost energy in the system due to system losses such as hydraulic friction, fluid leakage in PM_1 or PM_2, etc. Control of the system can be achieved by varying the displacements in the PM_1-shaft-PM_2 assembly (the hydraulic transformer).

The use of a hydraulic transformer with variable displacement PMs for motion control of hydraulic actuation is also used by Hung and Kwan (2008), but not in regards to an elevator. Although their motion control method contains similarities to the system introduced herein, key differences introduced in the proposed application to a hydraulic elevator are present. Principally, in the absence of losses, an external power source is eliminated and thus the system becomes driven exclusively by its pre-charged accumulators. A hydraulic pump driven by an EM acts as the main source of power input into Hung's system. Secondarily, in a typical implementation of the hydraulic transformer, the PMs share a pressure node, as shown in Hung's work. By eliminating this hydraulic communication, a versatile operation arises which includes freely designing for pressure differentials and flow through each individual PM, thus allowing for their most efficient use.

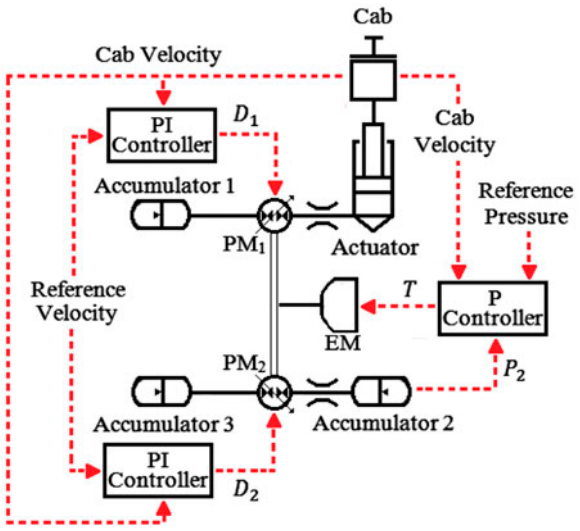

Figure 2. Introduced architecture and accompanying controllers.

The proposed architecture can operate in two different modes, which in summary reduce to Accumulator 2 providing power to lower the cab, hereafter referred to as Mode 1, or Accumulator 2 providing power to lift the cab, hereafter referred to as Mode 2. In Mode 1, cylinder extension is achieved by utilizing Accumulator 1 as the power source while energy is stored in Accumulator 2 via PM_2 working as a pump powered by PM_1 (itself acting as a motor). Cylinder contraction is achieved by utilizing Accumulator 2 as the main power source to drive PM_2 which, in turn, powers PM_1 and pumps fluid from the actuator to Accumulator 1, thereby lowering the cab and recharging Accumulator 1. In Mode 2, cylinder extension is achieved by utilizing Accumulator 2 to drive PM_2 (as a motor), which in turn drives PM_1 to pump fluid from Accumulator 1 to the actuator, thereby raising the cab. Cylinder contraction is achieved by letting the gravitational potential energy of a lifted cab to drive PM_1 (as a motor), which in turn drives PM_2 (as a pump) and thereby recharges Accumulator 2. Figure A2 in the Appendix introduces a visual depiction of the energy flow through the architecture in each mode. In either mode described above, the variable displacement that characterizes the PMs allows the torque to vary across the shaft as a function of the two displacements, thereby acting as an efficient and controllable speed governor.

4. Analytical model

Hydraulic circuits are inherently nonlinear due to the nonlinear relationship between differential pressure and flow in many hydraulic components. Specifically, for this system, gas-charged accumulators and the damping effects of the fluid conduits (tubing, valves, etc.) are both nonlinear. Due to the complexities that arise from the nonlinearity when obtaining mathematical models, a representation of the system using linear components, such as the spring-loaded accumulator and linear hydraulic resistances, are used in developing the control scheme. A fully nonlinear simulator in Section 5 tests the efficacy of the developed controllers.

The following equations describe the relationship between differential pressure and flow in the linear accumulator, and hydraulic resistance of a conduit, respectively,

$$\Delta P = P_0 + k \int q \, \mathrm{d}t \tag{1}$$

$$\Delta P = cq \tag{2}$$

where q denotes volumetric flow, ΔP the differential pressure, P_0 the precharge/initial pressure in the accumulator,

c the damping coefficient, and k the energy storage coefficient of an accumulator. The damping coefficient, c, represents all sources of losses due to flow resistance, such as valves, the hydraulic cylinder, and piping.

Additionally, the relationship between the torque, T, and pressure differential across a PM is given by,

$$\Delta P = \frac{T \pm T_{\text{fr}}}{D} \tag{3}$$

where T_{fr} denotes the friction torque for which the sign depends on whether the PM is motoring (positive) or pumping (negative); D refers to the displacement of the PM, which is given by the combination of q and leakage losses, q_{L}, divided by the angular velocity of the shaft, ω, as given in (4). Leakage losses change sign depending on whether the PM is motoring (negative) or pumping (positive),

$$D = \frac{q \mp q_{\text{L}}}{\omega} \tag{4}$$

To derive state equations, this work invokes an electric circuit approach and the concept of through and across variables, q and ΔP, respectively. In complete analogy to an electric circuit, the variable q remains constant through all pressure nodes in series while a pressure differential is associated with flow across each component. By determining the pressure nodes of the system (at each end of every hydraulic component), the relationships given by (1)–(3) between differential pressure and flow across each component, as shown in Figure 3, serve to derive the governing equations for both the top and the bottom hydraulic circuits.

Using the hydraulic equivalent of Kirchhoff's loop law, one can arrive at (5) and (6) for the top and bottom fluid domains, respectively:

$$P_1 - \Delta P_{\text{PM}_1} - \Delta P_{\text{c}_1} - P_{\text{cylinder}} = 0 \tag{5}$$

$$P_3 + \Delta P_{\text{PM}_2} - \Delta P_{\text{c}_2} - P_2 = 0 \tag{6}$$

Using Newton's 2nd law on the cab of mass m, and recognizing that $\frac{1}{A}\frac{\text{d}q_1}{\text{d}t}$ gives the acceleration of the cab, one finds an expression for P_{cylinder},

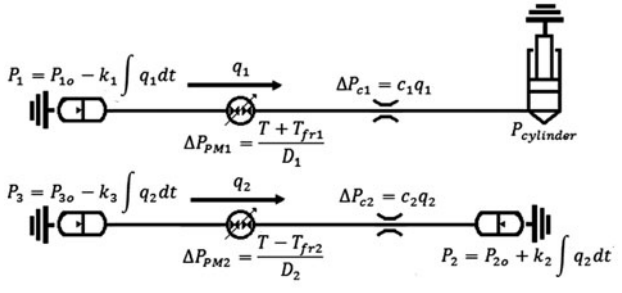

Figure 3. Hydraulic circuit representation of top and bottom fluid domains.

$$P_{\text{cylinder}} = \frac{m}{A^2}\frac{\text{d}q_1}{\text{d}t} + \frac{mg}{A} \tag{7}$$

Furthermore, by reasonably neglecting shaft inertia torques in comparison to PM inertias, the torque experienced by both PM's is assumed equal. Using this relationship and recognizing that the flows (q_1, q_2) are related by the angular speed of the shaft and the PM displacements $\left(\frac{q_2+q_{\text{L}_2}}{D_2} = \frac{q_1-q_{\text{L}_1}}{D_1}\right)$, one arrives at a single-input single-output (SISO) model of the system, with pressures as indicated in Figure 3, where the input is the ratio of displacements $\frac{D_2}{D_1}$ and the output is the flow q_1, which directly relates to the cab velocity by the area, A:

$$\begin{aligned}\frac{m}{A^2}\frac{\text{d}q_1}{\text{d}t} + \left(c_1 + \left(\frac{D_2}{D_1}\right)^2 c_2\right) q_1 + k_1 \int q_1 \, \text{d}t \\ + \frac{D_2}{D_1}(k_2 + k_3) \int \frac{D_2}{D_1} q_1 \text{d}t \\ = P_{1\text{o}} - \frac{mg}{A} - \frac{D_2}{D_1}(P_{2\text{o}} - P_{3\text{o}}) + \left(\frac{T_{\text{fr}_2} + T_{\text{fr}_1}}{D_1}\right) \\ + c_2 \frac{D_2}{D_1}\left(\frac{D_2}{D_1} q_{\text{L}_1} - q_{\text{L}_2}\right) + (k_2 + k_3)\frac{D_2}{D_1} \int q_{\text{L}_2} \text{d}t \\ + (k_2 + k_3)\frac{D_2}{D_1} \int \frac{D_2}{D_1} q_{\text{L}_1} \text{d}t\end{aligned} \tag{8}$$

Note that the time dependence of control input $\frac{D_2}{D_1}$ in the integral terms prevents expressing (8) as an equivalent second-order system through the usual change of variable. Figure 3 depicts the operation of the system in Mode 1; therefore, the corresponding derivation of (8) is also done for Mode 1. The system in Mode 2 would yield similar equations and the SISO nature would remain unaltered.

The input control variable shown by the analytical analysis of this system is a ratio of two independent inputs, D_1 and D_2. This translates to a non-uniqueness whereby an infinite number of combinations of D_1 and D_2 exist such that the speed of the cab is adequately controlled. This also implies that, should one of the PMs have a fixed displacement, the system remains completely controllable within a finite range of speeds. This, together with the two modes introduced previously, results in a flexible architecture with many choices for control and operation design.

Although the linear model described by (8) does not capture the non-linearity inherent to the hydraulic system, it remains useful in the determination of preliminary control strategies. In this case, using (8), a linear simulation of the system is built using Matlab's Simulink environment wherein the input to the plant is either D_1 or D_2 (while the other holds constant) and the output is the cab velocity. This allows for the design of preliminary proportional-integral (PI) linear feedback controllers used to control the displacements of the PMs. The controller gains determined in the preliminary design are then tuned as needed to ensure appropriate operation of the

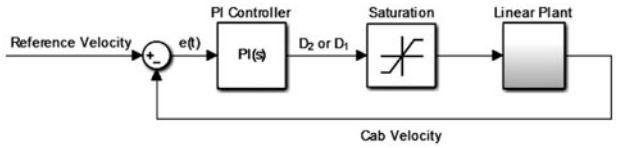

Figure 4. Block diagram of PM controllers as applied to the linear model.

non-linear model, introduced in Section 5. Characteristic to the feedback PI controller, the command signal generated depends on the error signal $e(t)$, as defined in Figure 4, and is of the form,

$$D_n(t) = P_n e(t) + I_n \int e(t)\mathrm{d}t \tag{9}$$

where $n = 1, 2$ to refer to the corresponding PM (PM_1 or PM_2) and P and I denote controller gains. The command signal $D_n(t)$ passes through a saturation block to limit minimum and/or maximum values of the signal as needed; the use of these saturation blocks will be further explored in Section 5 in the context of efficiency. Future use of the analytical equations introduced by (8) could entail designing more advanced control strategies such as trajectory tracking or the use of Dynamic Programming to optimize the command signal $D_n(t)$ for efficiency (Bellman 1957, Singhose and Seering 2011).

5. Control and efficiency considerations

To test the control efficacy and to determine the system's energy efficiency, a high-fidelity numerical model of the system is built using Matlab's Simulink/Simscape environment (Chaturvedi 2010), as depicted in Figure 5. Using the SimHydraulics tools within Simscape, the model incorporates the non-linearities neglected in the linear model by using the provided hydraulic component building blocks. Furthermore, functionality for the testing of various scenarios is also built in, such as a varying cab load (i.e. passengers), varying cab travel heights, varying travel speeds, etc.

The numerical model uses the built-in (nonlinear) SimScape gas-charged accumulator block for Accumulators 1, 2, and 3, and the SimScape variable-displacement hydraulic machine block to model the PMs. The losses in the system arising from hydraulic flow are modeled using non-linear hydraulic resistances, as shown, for each fluid domain. Finally, an ideal torque source block models the EM.

The variable-displacement hydraulic machines take as inputs a control signal for their displacements D_1 and D_2 generated via (9) and saturated so as to limit the maximum value of the signal to the maximum attainable value of displacement for the corresponding PM. Additionally, $D_1(t)$ is also limited to a minimum displacement command, thereby giving preference to commanding

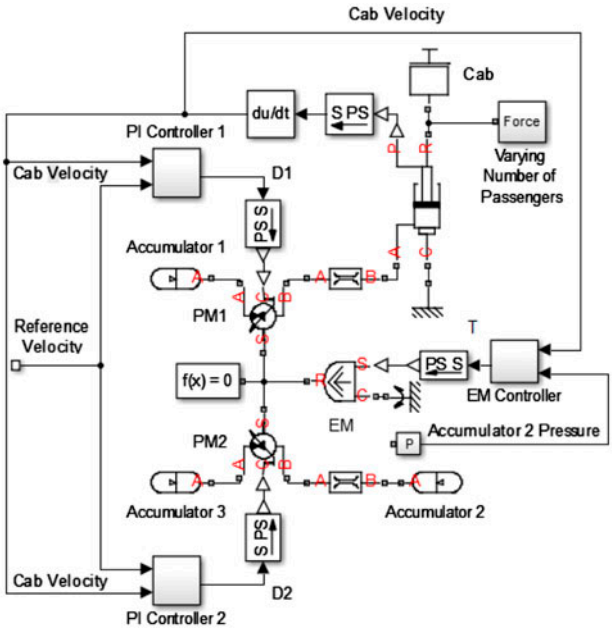

Figure 5. Simulink/SimScape hydraulic elevator model.

PM_2, which ensures a more efficient operation, explained in detail later. Prior to reaching the SimScape block, the saturated signals coming from PI controllers 1 and 2, in Figure 5, are processed through the *SPS* blocks shown; the *SPS* blocks take a *Simulink* signal and convert it into a *Physical* signal able to be used by the SimScape variable-displacement hydraulic machine block.

The EM overcomes parasitic losses and compensates for energy temporarily lost by people ascending and then exiting the cab. In detail, the EM provides input energy during the descent of the cab while its output is suppressed during the ascent. This is done by feeding the cab velocity back into the EM and suppressing its output when the cab velocity is greater than zero (during ascent). A controller of the form of (9) again governs; however, the integral component is eliminated, which serves to avoid integrator windup during the time the controller output is suppressed. The EM compensates for any energy loss in the system; it does so by ensuring that enough energy (expressed as a fixed reference pressure) in Accumulator 2 always remains to drive a full cab back up to the top floor. The control strategy described was decided upon after assessing the efficiency of several possible control strategies, the process of which will now be described.

The system has four basic Control Operations: (1) using Mode 1, wherein Accumulator 2 provides power to lower the cab, while primarily controlling on D_1, (2) using Mode 1 while primarily controlling on D_2, (3) using Mode 2, wherein Accumulator 2 provides power to raise the cab, while primarily controlling on D_1, and (4) using Mode 2 while primarily controlling on D_2. To determine which operation to pursue, a simple analysis of the total system energy is performed. In Mode 1, for

a given cab gravitational potential energy E_{cab}, the energy provided by Accumulator 1 (E_1) needs to both lift the cab and store sufficient energy E_2 in Accumulator 2 to return the cab back down. In the absence of losses, and neglecting the energy storage capacity of the low-pressure accumulator (Accumulator 3), the relationship becomes (10), where E_{tot} is the total energy *transfer* through the system for a given E_{cab}.

$$E_{cab} + E_2 = E_1 = E_{tot} \tag{10}$$

In Mode 2, both the energy provided by Accumulator 1 plus the energy provided by Accumulator 2 must suffice to lift the cab, while on the return, the gravitational potential energy of the cab divides into Accumulator 1 and Accumulator 2. In the absence of losses, and neglecting the energy storage capacity of Accumulator 3, the relationship (11) follows.

$$E_1 + E_2 = E_{cab} = E_{tot} \tag{11}$$

Figure A2 can again be referenced for a visual representation of the energy flows described by (10) and (11). Comparing (10) and (11), it becomes apparent that for the same given cab energy required (i.e. E_{cab} in both equations), E_{tot} will be less in Mode 2. This translates into a lower net energy loss in Mode 2 than in Mode 1, which points to Control Operation (3) and Control Operation (4) as more desirable. To further narrow down to the most desirable Control Operation, a closer look at the individual energy transfer of each PM is considered.

A variable displacement PM tends to have a reduced efficiency at small displacements (Lumkes *et al*. 2009). This implies that in Control Operation (3), PM_1 operates less efficiently, while in Control Operation (4), PM_2 operates less efficiently. While PM_2 transfers only the energy flowing in and out of Accumulator 2, PM_1 transfers both the energy associated with Accumulator 1 and that associated with Accumulator 2. From this one can conclude that controlling on D_2 will result in lower net energy loss than controlling on D_1, and therefore Control Operation (4) emerges as the most desirable.

Within Control Operation (4), further necessary choices arise due to the non-uniqueness posed by the presence of controllable D_1 and D_2. One reasonable choice controls exclusively on D_2 while setting D_1 to ensure that PM_1, which transfers the most energy and thus subjects the system to its greatest losses, operates at its highest efficiency. A second choice controls both D_1 and D_2 using efficiency considerations of each PM. While this choice results in lowering of the operating efficiency of the high-energy transferring PM_1, large gains can be achieved in the operating efficiency of PM_2, potentially resulting in an overall higher system efficiency than had just D_2 been controlled. Additionally, increasing the displacement at which PM_2 operates can mitigate some of the noise associated with operating a PM at low displacements (Manring 2003). To determine which choice results in better efficiency, a detailed analysis of the operating efficiency of the PM's becomes necessary. Note that future work may consider the optimal control problem in which no a priori strategy is assumed for control of D_1 and D_2, and instead techniques such as Dynamic Programming are used, together with a given load cycle, to determine optimal trajectories of D_1 and D_2 through the control space. This is considered beyond the scope of the present paper.

To begin, the losses in a PM are characterized as a function of the differential pressure across the PM, the displacement of the PM and the angular velocity of the shaft. The losses can generally be described as losses due to leakage (volumetric losses), q_L, which tend to account for large parts of the inefficiency (Wang 2012), and losses due to friction of rotation (mechanical losses), T_{fr}, both of which are approximated by the following equations, given by Hicks and Edwards (1971), and incorporated into the appropriate simulation blocks of the SimScape model.

$$q_L = D\omega k_{L_1}\left(\frac{\Delta P}{\Delta P_{nom}}\right)^{k_{LP}}\left(\frac{D}{D_{max}}\right)^{k_{LD}}\left(\frac{\omega}{\omega_{nom}}\right)^{k_{Lm}} \tag{12}$$

$$T_{fr} = D\Delta P k_{F_1}\left(\frac{\Delta P}{\Delta P_{nom}}\right)^{k_{FP}}\left(\frac{D}{D_{max}}\right)^{k_{FD}}\left(\frac{\omega}{\omega_{nom}}\right)^{k_{Fm}} \tag{13}$$

In these relationships all k coefficients are empirically derived through testing of the PM unit. Here, the values of k are experimentally determined for an Eaton/Linde Duraforce PM as reported in Pei (2012).

The PM also has mutually exclusive modes of motoring and pumping. The efficiency of the unit as a function of the losses (leakage and friction) differs for both modes. Equations (14) and (15) encompass the effect of the different modes. The variable n differentiates the motoring mode ($n = -1$) vs. the pumping mode ($n = 1$),

$$q = D\omega - nq_L \tag{14}$$

$$T = D\Delta P + nT_{fr} \tag{15}$$

thus the volumetric efficiencies in both the pumping and motoring mode, η_{mp} and η_{mm}, and the mechanical efficiencies in both the pumping and motoring mode, η_{vp} and η_{vm}, become,

$$\eta_{mp} = \frac{D\Delta P}{D\Delta P + T_{fr}},\ \eta_{mm} = \frac{D\Delta P - T_{fr}}{D\Delta P} \tag{16}$$

$$\eta_{vp} = \frac{D\omega - q_L}{D\omega},\ \eta_{vm} = \frac{D\omega}{D\omega + q_L} \tag{17}$$

In each mode, the total efficiency results from the product of both the volumetric efficiency and the mechanical efficiency. Finally, the dependence of the PM efficiency on three operating variables (D, ω, and ΔP) warrants some simplifications. Figures A3 and A4 in the Appendix provide the efficiency contours of the PM while holding displacement constant and differential pressure constant, respectively. From these two figures one can conclude that the PM efficiency varies little with

changes in angular velocity. In light of this, for a particular operation, maintaining a constant ω and examining the efficiency as the other two variables vary satisfactorily describes the efficiency of the PM.

Equations (12)–(17), together with the simplification of holding ω constant, are used to examine the efficiency of both PM's while either (a) D_2 is exclusively controlled, or (b) both D_1 and D_2 are controlled. Table A1 in the Appendix provides the parameter inputs for the nonlinear model depicted in Figure 5, including the pertinent values for the reference motion profile and the reference pressure signal. Simulations are performed which extend the actuator a distance of 14.6 m and retract it the same amount, under a load of 2080 kg. Figure 6 depicts the operating points for the PM's using both control strategies to achieve this movement. Note that contours indicate PM efficiency. When controlling exclusively on D_2, PM_1 operates most efficiently (since it maintains its maximum displacement); however, PM_2 reaches an efficiency as low as 70%. Alternatively, controlling both displacements allows for significant improvements in the operating efficiency of PM_2 at the cost of a lower operating efficiency of PM_1. Due to this inherent tradeoff, the control approach which yields greater efficiency requires further evaluation.

For a typical hydraulic elevator, an analysis of the total actuation efficiency of the system (calculation is described in detail in Section 6) with both control strategies is shown in Figure 7. Here, one can clearly see improvement in efficiency when controlling on both D_1 and D_2, particularly when the cab carries a lower payload.

These results allowed the design of the final heuristic control strategy: control on both D_1 and D_2 wherein higher authority is given to D_2 control by limiting the minimum value of the D_1 control signal. This ensures that PM_1, which transfers the most energy, does not operate below a minimum efficiency.

Figure 8 depicts output from the nonlinear simulator displaying the ability of the architecture and the selected control strategy to accurately position the cab through a given schedule of floors (4th-1st-3rd-2nd-3rd-1st) using a desirable velocity profile and a load of 2080 kg (corresponding to a full cab). The bottom subfigure depicts simulation results for commanded and obtained velocity as the cab moves up through a single floor. Note that these results provide evidence that the elevator system successfully navigates the schedule of floors while the control strategy accurately tracks the reference velocity profile.

6. Efficiency and energy consumption comparison

An efficiency comparison of both the system introduced herein, heretofore referred to as the present system, and a recent electrohydraulic system (Moser 2005, Yang *et al*. 2007) depicted in detail in Figure A1 allows one to assess the performance and merits of the present

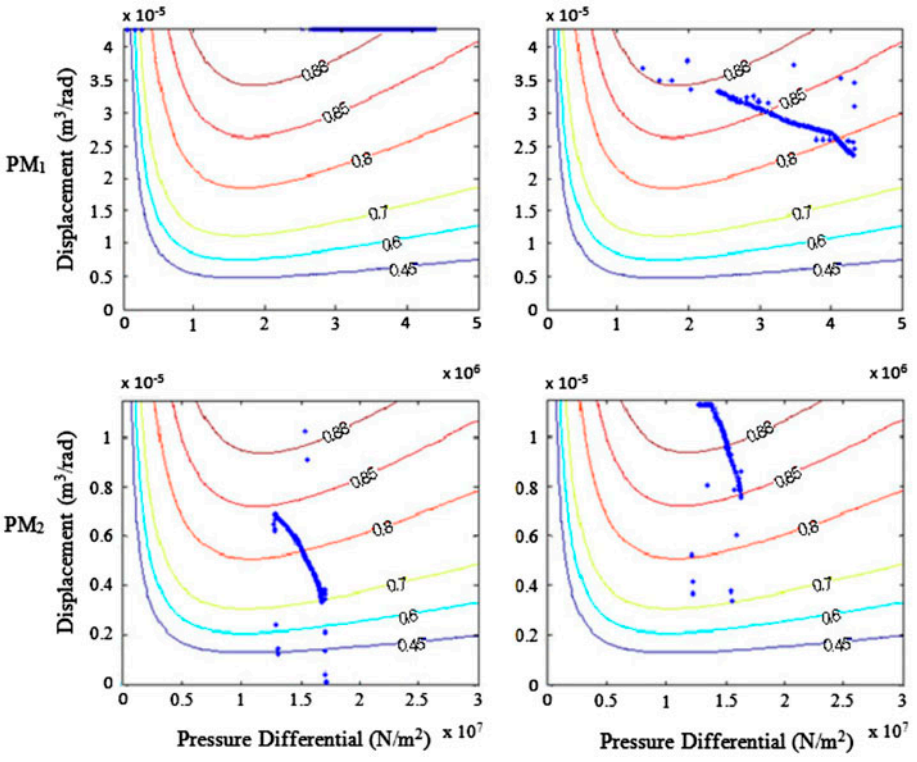

Figure 6. Contrast of operating regions of each PM when only PM_2 displacement is controlled (left subfigures) and when both PM_1 and PM_2 displacements are controlled (right subfigures).

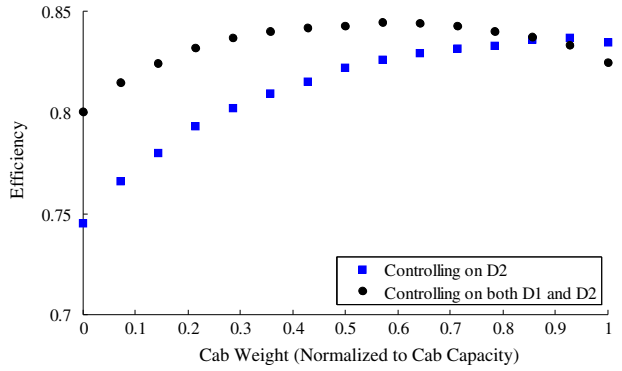

Figure 7. Comparison of control strategies as pertains to actuation efficiency.

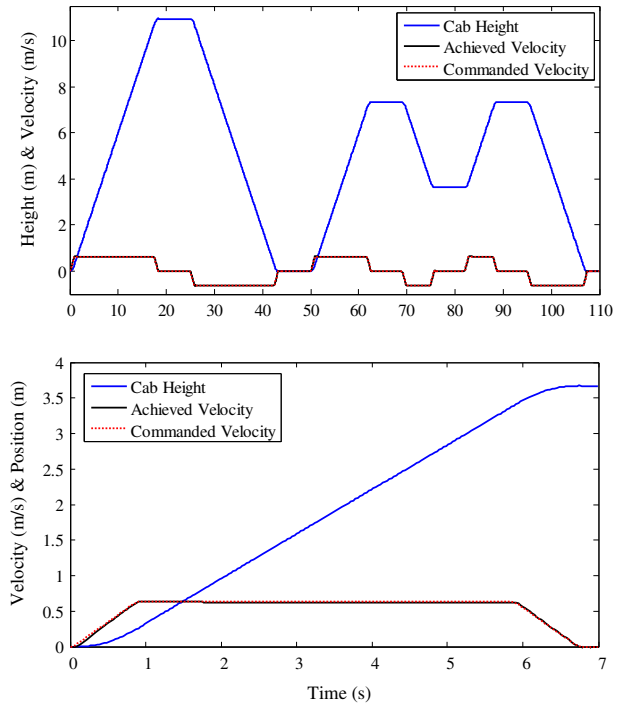

Figure 8. Simulation results for the introduced architecture controlled for velocity through a schedule of floors (top); details of simulated motion moving up through a single floor (bottom).

system. The electrohydraulic system incorporates a bi-directional pump/motor driven by an EM with both generator and motoring functionality. The EM siphons off power from the system when the direction of flow is from a high pressure to a low pressure, which is then either fed back to the grid or stored in a battery. When the direction of flow is from a low pressure to a high pressure the EM provides power to the system from the grid or the battery. Figure A5 in the Appendix depicts a SimScape model built for the electrohydraulic system. The components shared by both systems are sized identically so as to ensure comparability. Table A2 in the Appendix tabulates the system parameters, including the EM controller; the present system uses the parameters previously tabulated in Table A1.

The actuation efficiency of both systems is calculated at each payload level, ranging from an empty cab (1100 kg) to a full cab (14 people, 2080 kg); an average of 70 kg is used per person. Fifteen simulations are performed, one for each payload level, of the cab traveling to the 4th floor and returning back down. The total system actuation efficiency, governed by the individual efficiencies of the components, is calculated as a ratio of energy recovery (E_{out}) to energy expenditure (E_{in}). The energy storage capacity of Accumulator 3 is again neglected as well as energy losses associated with Accumulators 1 and 2. Energy losses in hydraulic accumulators are primarily due to the heat exchange that occurs between the gas and the pressure vessels; in much less measure, friction losses within the accumulator also contribute. A properly designed accumulator can severely mitigate heat exchange losses and achieve an efficiency rating of up to 95% (Pourmovahed *et al.* 1988).

For the present system during ascent, E_{in} is primarily provided by Accumulator 1 and Accumulator 2 while the gravitational potential energy stored in the cab (E_{cab}) is used for E_{out}. Thus, the total efficiency of the system when the cab ascends follows as,

$$\eta_{\text{system1}} = \frac{E_{\text{out}}}{E_{\text{in}}} = \frac{E_{\text{cab}}}{E_1 + E_2} \tag{18}$$

During descent, the auxiliary EM will begin to input energy into the system, the gravitational potential energy adds to this input, while the output energy is that entering both accumulators through the descent. The efficiency of the system while descending then follows as,

$$\eta_{\text{system1}} = \frac{E_{\text{out}}}{E_{\text{in}}} = \frac{E_1 + E_2}{E_{\text{cab}} + E_{\text{EM}}} \tag{19}$$

In the electrohydraulic system, an accumulator, operating as the hydraulic counterweight, acts as a continuous power source to the cab. An EM coupled with a PM adds or subtracts power as needed to maintain a desired velocity profile. In the case where energy is subtracted, a battery stores the energy and later returns it to the system. The efficiency of the accumulator associated with this system is also neglected so as to maintain comparability. The energy conversion efficiency of the battery, η_{battery}, conservatively estimated at 75%, applies both when charging and depleting the battery.

On the ascent, E_{in} in the electrohydraulic system equals energy provided by its accumulator, the EM, and the battery, while E_{out} is the gravitational potential energy.

$$\eta_{\text{system2}} = \frac{E_{\text{out}}}{E_{\text{in}}} = \frac{E_{\text{cab}}}{E_{\text{accumulator}} + E_{\text{EM}} + E_{\text{battery}}} \tag{20}$$

On the descent, E_{in} is the gravitational potential energy while E_{out} equals the energy into the accumulator plus the energy supplied to the battery.

$$\eta_{\text{system2}} = \frac{E_{\text{out}}}{E_{\text{in}}} = \frac{E_{\text{accumulator}} + E_{\text{battery}}}{E_{\text{cab}}} \tag{21}$$

The energy leaving or entering an accumulator over time is determined by the time integral of the product of the pressure and flow through the pressure node associated with the accumulator, or:

$$E_{\text{accumulator}} = \int Pq\mathrm{d}t \tag{22}$$

Similarly, the energy provided by the EM is the integral of the product of its torque T, and its speed ω given by:

$$E_{\text{EM}} = \int T\omega\mathrm{d}t \tag{23}$$

The ideal torque source employed to model the EM does not capture the loss characteristic of an EM; because of this, post processing of the results incorporates the losses. The losses of an electric motor in operation, as a function of the torque T, and the angular velocity of the shaft ω, are approximated by the following equation (Larminie and Lowry 2012):

$$P_{\text{losses}} = k_{\text{c}}T^2 + k_{\text{i}}\omega + k_{\omega}\omega^3 + C \tag{24}$$

These losses arise due to electrical resistance of the wires in the motor, $k_{\text{c}}T^2$, due to the magnetic effect on the iron of the motor, $k_{\text{i}}\omega$, due to friction and windage, $k_{\omega}\omega^3$, and due to components of the motors that operate at all times, C. The different k coefficients and the value of C are generally provided by the manufacturer of the electric motor. This paper uses coefficients from those given in Larminie and Lowry (2012). Using this relationship for losses the efficiency for the EM in both motor and generator modes can be calculated by (24) and (25), respectively, as follows:

$$\eta_{\text{m}} = \frac{P_{\text{out}}}{P_{\text{in}}} = \frac{P_{\text{out}}}{P_{\text{out}} + P_{\text{losses}}} = \frac{T\omega}{T\omega + k_{\text{c}}T^2 + k_{\text{i}}\omega + k_{\omega}\omega^3 + C} \tag{25}$$

$$\eta_{\text{g}} = \frac{P_{\text{out}}}{P_{\text{in}}} = \frac{P_{\text{in}} - P_{\text{losses}}}{P_{\text{in}}} = \frac{T\omega - k_{\text{c}}T^2 - k_{\text{i}}\omega - k_{\omega}\omega^3 - C}{T\omega} \tag{26}$$

where P_{out} represents power output and P_{in} represents power input of the EM.

Using (18)–(26), a complete analysis of the actuation efficiency is performed. Pressures, flows, torque, shaft speed, cab height, and cab velocity are all recorded throughout simulations. Figure 9 reports the actuation efficiency as it varies with the cab payload for both systems.

With an empty cab, the electrohydraulic system has higher actuation efficiency. This high efficiency results from a low participation of the EM since the accumulator provides the majority of the energy during actuation. However, when the cab weight reaches approximately one fifth of its maximum weight (corresponding to three people in the cab), the present system begins to gain an advantage, improving by up to 13% when the cab carries a full payload.

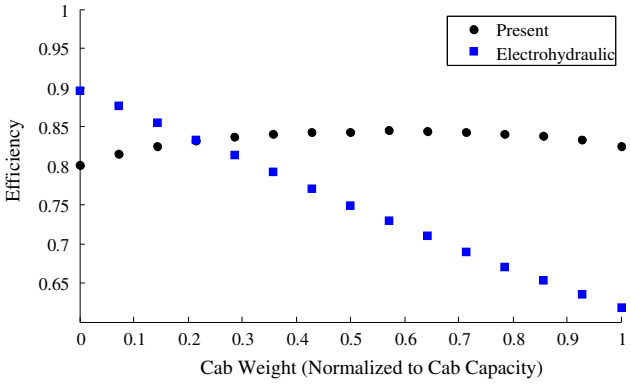

Figure 9. Efficiency during operation as a function of cab load.

While the efficiency of actuation proves useful, the typical elevator consumer makes purchasing decisions based more on the net energy (and its cost) usage for a given system. A discussion of the energy usage characteristics from the present architecture is first realized before providing a comparison between it and the electrohydraulic system. Figure 10 depicts the pressure of all accumulators in the present architecture while the simulator moves 50 persons.

In the figure, the cab performs four trips to bring the 50 persons up to the 4th floor. A trip here refers to the cab going up to the desired floor and then returning to the ground floor. Should people be descending, the cab ascends empty (1100 kg), and descends with the specified load. Should people be ascending, as is the case in Figure 10, the cab ascends with the specified load and descends empty. To bring 50 people up to the 4th floor, the cab performs three trips while carrying 14 persons,

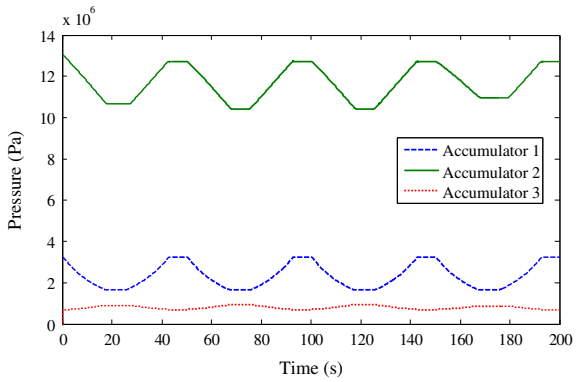

Figure 10. Accumulator pressures in the system while 50 people are brought up to the 4th floor; full cab capacity.

and one trip while carrying 8. As per the designed operation of the system, Accumulator 2 depletes while the cab ascends, and recharges using the cab potential energy and the EM when descending. The EM ensures that Accumulator 2 always reaches a desired pressure when the cab is fully down, as can be seen in the figure. Note that on the last trip the pressure drop of Accumulator 2 is noticeably less than the other three. This occurs since on the fourth trip, the elevator only carries 8 persons up, and therefore Accumulator 2 releases less energy. This also translates into less energy input from the EM since the energy lost from 8 people ascending is less than that from 14 people ascending. It then follows that an empty cab ascending to bring people down will require even less energy input from the EM. Figure 11 depicts such a scenario.

In Figure 11 the energy input into the system required to move 50 persons up to the fourth floor (ascent) is contrasted with that required to bring 50 persons down from the fourth floor (descent). Energy input is calculated from (23). In both cases, the cab executes four trips as described previously. Note that, as per the control strategy described previously, the energy input increases only during the descent of the cab (corresponding to periods of EM operation). From the figure, it becomes clear that people descending will require less energy input into the system. This introduces a characteristic of the system that results in a period of high energy consumption (people ascending) and a period of low energy consumption (people descending); which may be favorable in some applications such as integrating the power supply with renewable power sources (photovoltaic cells) whose period of maximal power generation may coincide with periods of high energy consumption (i.e. commercial applications in which people ascend during daylight hours).

With the energy consumption characteristics of the system now described, a comparison (of the energy consumption) between the present system and the electrohydraulic system is now introduced. Recording the system energy input, E_{EM}, in both systems for a full day operation of the elevator provides the necessary data for the comparison. A full day for this comparison entails 50 persons, per floor, descending, and then ascending. Both of the systems are simulated in a four floor building, which implies a total of 150 persons being moved (1st floor is bottom floor). For a day's period, a minimum cab load (one person) entails simulating the cab as it brings all 150 persons, up and down, one-by-one. Similarly, a full cab load (14 persons) entails the cab carrying 14 persons, unless there are less than 14 persons remaining on a floor, at which point the cab carries the remaining; this was introduced previously in the simulations performed for Figures 10 and 11. For easier reference, Figure A6 in the Appendix depicts a full day operation for a cab load of 13 people for one floor. With these definitions for a full day, the cab performs a total of 300 trips at its minimum cab capacity: 50 trips to move persons up and 50 trips to move them down for a total of 100 trips per floor beyond the 1st floor (bottom floor). Accordingly, at its maximum capacity the cab performs a total of 24 trips (eight per floor). Table A3 in the Appendix tabulates the total trips for a full day at each cab load. It therefore follows that for both systems a minimum cab capacity, although actuated highly efficiently (electrohydraulic system), requires more net energy input than running a consistently full cab due to the larger number of trips required. Figure 12 depicts the daily energy input as a function of the cab weight (ranging from 1 person to 14 persons) used for the full day simulation, together with results for the electrohydraulic architecture.

Similar to the actuation efficiency results presented earlier, the present system tends to gain an advantage as the cab payload increases, reaching as high as a 23% reduction in daily input energy over the electrohydraulic system. The comparison of both systems yields results in favor of the present system introduced. For low occupancy rates, the present system falls short in both actuation efficiency and daily input energy; however, when the cab transports more than two or three people per trip, the present system gains advantages in both measures. Many elevator applications meet this condition, particularly in residential and commercial applications where the majority of the people traffic occurs at the beginning and end of the day. The present

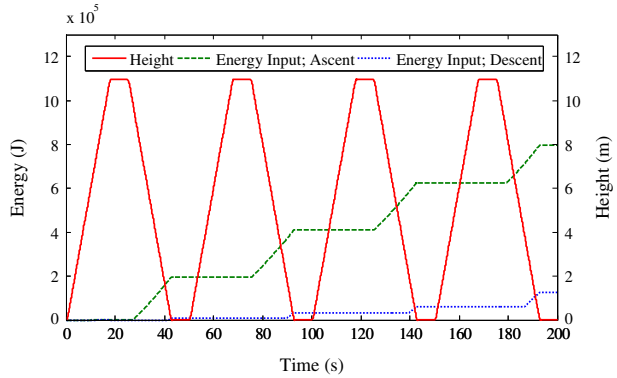

Figure 11. Energy input required to move 50 persons up (ascent) and 50 persons down (descent) from the 4th floor.

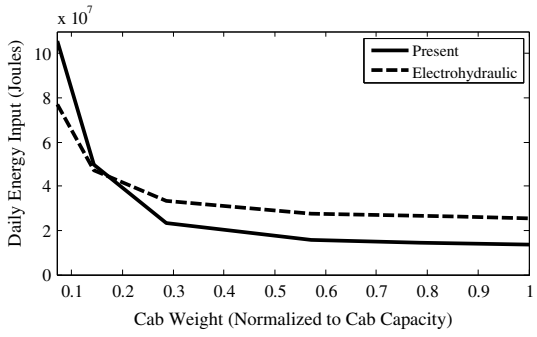

Figure 12. Daily input energy as a function of cab payload.

system also benefits from relative simplicity since it incorporates its own energy storage devices, as opposed to the electrohydraulic system which requires power electronics and batteries, or a means to return electrical energy to the grid.

7. Conclusions

A hydraulic architecture has been introduced for speed control and energy regeneration in a hydraulic elevator system. In the absence of losses, the system makes use of a specialized form of a hydraulic transformer to achieve a self-sufficient energy flow exclusively using pre-charged accumulators and provides functionality for motion control via variable displacement hydraulic pump/motors. Governing equations were derived for a simplified version of the system, exposing non-uniqueness in the independent control. Exploitation of this non-uniqueness allowed for efficient control of the system using simple PI controllers. In practical application, the new architecture requires a small external power source (e.g. an electric motor) to overcome component losses. Simulation results using a high-fidelity, nonlinear simulator demonstrate the effectiveness and efficiency of the architecture. In comparison to similar simulation results for a recently introduced electrohydraulic system, the introduced architecture exhibited up to a 13% increase in actuation efficiency and a 23% decrease in daily input energy over a typical usage cycle. These results suggest that the new architecture may be attractive for continued exploration.

Nomenclature

ΔP	Pressure differential across a component
P_0	Initial pressure in an accumulator
k	Energy storage coefficient of an accumulator
q	Fluid flow
c	Fluid damping coefficient
T	Shaft torque
T_{fr}	Frictional torque
D	PM displacement
ω	Shaft speed
q_{L}	Leakage flow
P_{cylinder}	Pressure at cap side of hydraulic cylinder
P	Pressure in accumulator
m	Cab mass
A	Cross-sectional area of cap side of hydraulic cylinder
g	Gravitational acceleration
I	Integral gain of feedback controller
P	Proportional gain of feedback controller
e	Error signal associated with feedback controller
E_{cab}	Energy provided to or by elevator cab
E_2	Energy provided to or by Accumulator 2
E_1	Energy provided to or by Accumulator 1
E_{tot}	Total energy flow through the system
k_{L_l}	Volumetric efficiency proportionality coefficient
ΔP_{nom}	Nominal pressure of PM
D_{max}	Maximum displacement of PM
ω_{nom}	Nominal shaft speed of PM
k_{LP}	Volumetric efficiency pressure coefficient
k_{LD}	Volumetric efficiency displacement coefficient
k_{Lm}	Volumetric efficiency angular velocity coefficient
k_{FP}	Mechanical efficiency pressure coefficient
k_{FD}	Mechanical efficiency displacement coefficient
k_{Fm}	Mechanical efficiency angular velocity coefficient
k_{F_l}	Mechanical efficiency proportionality coefficient
n	Machine type coefficient
η_{mp}	Mechanical efficiency while pumping
η_{mm}	Mechanical efficiency while motoring
η_{vp}	Volumetric efficiency while pumping
η_{vm}	Volumetric efficiency while motoring
η_{system1}	Total efficiency of present system
E_{out}	Energy flow out of hydraulic PM(s)
E_{in}	Energy flow into hydraulic PM(s)
E_{EM}	Energy flow out of EM
η_{system2}	Total efficiency of electrohydraulic system
$E_{\text{accumulator}}$	Energy provided to or by an accumulator
E_{battery}	Energy provided to or by a battery
P_{losses}	Power losses in EM
k_{c}	Electrical resistance efficiency coefficient
k_{i}	Magnetic loss efficiency coefficient
k_{ω}	Friction and windage efficiency coefficient
C	Miscellaneous loss constant
η_{m}	Efficiency of electric motor
P_{out}	Power output of EM
P_{in}	Power input of EM
η_{g}	Efficiency of electric generator

Funding

The authors gratefully acknowledge the National Science Foundation's Center for Compact and Efficient Fluid Power (NSF CCEFP) and the National GEM Consortium for financial support of the research described herein.

Notes on contributors

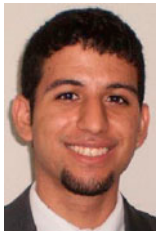

Oscar R. Peña is a graduate student and graduate research assistant in the George W. Woodruff School of Mechanical Engineering of the Georgia Institute of Technology. He received a B.S. in Civil and Environmental Engineering from the University of South Florida (2013). His graduate coursework focuses on dynamical systems and control theory and his research centers around hydraulic systems.

Michael J. Leamy is an associate professor in the George W. Woodruff School of Mechanical Engineering at the Georgia Institute of Technology, and a Fellow of the American Society of Mechanical Engineers. He received his B.S. from Clarkson University (1993), and his M.S., and Ph.D. (1995, 1998) from The University of Michigan, Ann Arbor, in Mechanical Engineering.

References

Bellman, R., 1957. *Dynamic programming*. Princeton, NJ: Princeton University Press.

Celik, F. and Korbahti, B., 2008a. Why hydraulic elevators are so popular? Part I. *Asansör Dünyasi* [Online]. Available from: http://www.blain.de/pdf/article/Why_hydraulic_elevators_are_so_popular-Part1.pdf.

Celik, F. and Korbahti, B., 2008b. Why hydraulic elevators are so popular? Part II. *Asansör Dünyasi* [Online]. Available from: http://www.blain.de/pdf/article/Why_hydraulic_elevators_are_so_popular-Part2.pdf.

Chaturvedi, D.K., 2010. *Modeling and simulation of systems using Matlab and Simulink*. London: Taylor and Francis Group.

Edwards, J.T., 1992. Conserving energy in oil hydraulic elevator system. *Elevator world*, 40 (7), 51–52.

Grabbel, J. and Ivantysynova, M., 2005. An investigation of swash plate control concepts for displacement controlled actuators. *International journal of fluid power*, 6 (2), 19–36.

Hicks, T.G. and Edwards, T.W., 1971. *Pump application engineering*. New York City: McGraw-Hill.

Hung, H.T. and Kwan, A.K., 2008. A study on the position control of hydraulic cylinder driven by hydraulic transformer using disturbance observer. *In*: S.K. Kim, ed. *International conference on control, automation and systems*. Seoul: IEEE, 2634–2639.

Larminie, J. and Lowry, J., 2012. *Electric vehicle technology explained*. New York City: Wiley.

Lumkes, J., Batdorff, M., and Mahrenholz, J., 2009. Model development and experimental analysis of a virtually variable displacement pump system. *International journal of fluid power*, 10 (3), 17–27.

Manring, N., 2003. Valve-plate design for an axial piston pump operating at low displacements. *Journal of mechanical design*, 125 (1), 200–205.

Manring, N.D., *et al.*, 2013. Increasing the power density for axial-piston swash-plate type hydrostatic machines. *Journal of mechanical design*, 135 (7), 071002.

Mitchell, J.P., 2001. *Load sensing hydraulic control system for variable displacement pump*. United States of America patent application 6216456 B1.

Moser, D., 2005. *Hydraulic elevator with an accumulator*. United States of America patent application 6957721 B2.

Oda, Y. and Shirai, K., 1997. *Displacement control system for variable displacement hydraulic pump*. United States of America patent application 5697764 A.

Pei, D., 2012. *Development of simulation tools, control strategies, and a hybrid vehicle prototype*. Thesis (Master). Georgia Institute of Technology.

Pourmovahed, A., *et al.*, 1988. Experimental evaluation of hydraulic accumulator efficiency with and without elastomeric foam. *Journal of propulsion*, 4 (2), 185–192.

Ran, L., 1998. *Study on a new type of speed control system and energy-saving in hydraulic elevator*. Thesis (PhD). Zhejiang University.

Shimoaki, M., 1992. Vvvf-controlled hydraulic elevators. *Mitsubishi electric advance*, 61, 13–15.

Singhose, W. and Seering, W., 2011. *Command generation for dynamic systems*. Atlanta, GA: William Singhose.

Ven, J.V.D., 2009. Increasing hydraulic energy storage capacity: flywheel-accumulator. *International journal of fluid power*, 10 (3), 41–50.

Verma, S., n.d. *Invention story of elevator* [Online]. Available from: http://www.Engineersgarage.Com/Invention-Stories/Elevator-History [Accessed 28 Jan 2015].

Wang, S., 2012. Improving the volumetric efficiency of the axial piston pump. *Journal of mechanical design*, 134 (11), 111001.

Wang, M. and Li, P. Y., 2012. Displacement control of hydraulic actuators using a passivity based nonlinear controller. *In*: *Dynamic systems and control conference joint with the motion and vibration conference*, 2012. Santa Clara, CA: ASME, 715–721.

Xia, J. and Durfee, W.K., 2013. Analysis of small-scale hydraulic actuation systems. *Journal of mechanical design*, 135 (9), 091001.

Xu, B., 2001. *Study on energy-saving control system of A Vvvf hydraulic elevator using hydraulic accumulator*. Thesis (PhD). Zhejiang University.

Xu, B., Jianjie, L., and Yang, H., 2003. Study on energy consumption characteristics of Vvvf controlled hydraulic elevators with pressure accumulators. *Chinese journal of mechanical engineering*, 39 (7), 63–67.

Xu, J., Zhang, B., and Lin, B., 2006. Energy consumption characteristics of vvvf controlled hydraulic elevators. *Chinese journal of mechanical engineering*, 42 (8), 137–141.

Yang, H., Sun, W., and Xu, B., 2007. New investigation in energy regeneration of hydraulic elevators. *IEEE/ASME transactions on mechatronics*, 12 (5), 519–526.

Zimmerman, J., 2008. *Design and simulation of an energy saving displacement-controlled actuation system for a hydraulic excavator*. Thesis (Master). Purdue University.

Zimmerman, J. D., *et al.*, 2007. Energy consumption of an LS excavator hydraulic system. *In*: *International mechanical engineering congress and exposition*, 2007. Seattle, WA: ASME, 117–126.

Zürcher, J. and Moser, D., 2003. *Hydraulic elevator, comprising a pressure accumulator which acts as a counterweight and a method for controlling and regulating an elevator of this type*. United States of America patent application 6506711 B1.

Appendix 1.

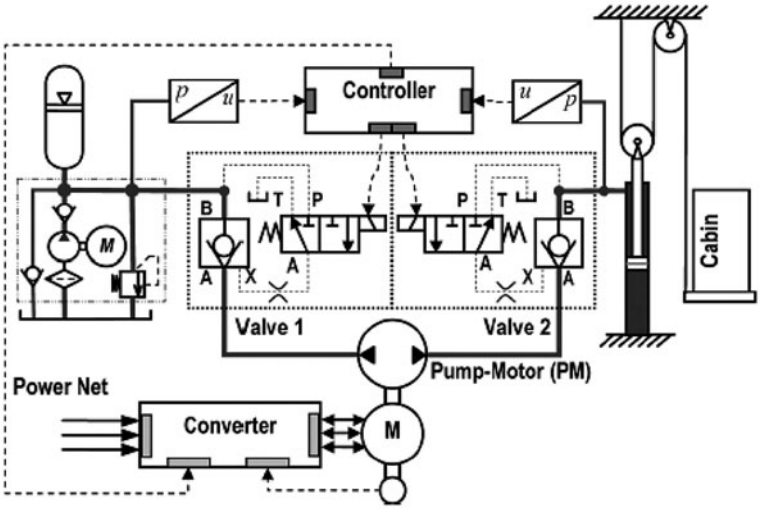

Figure A1. Electrohydraulic system patented by Bucher Hydraulics (Yang *et al*. 2007).

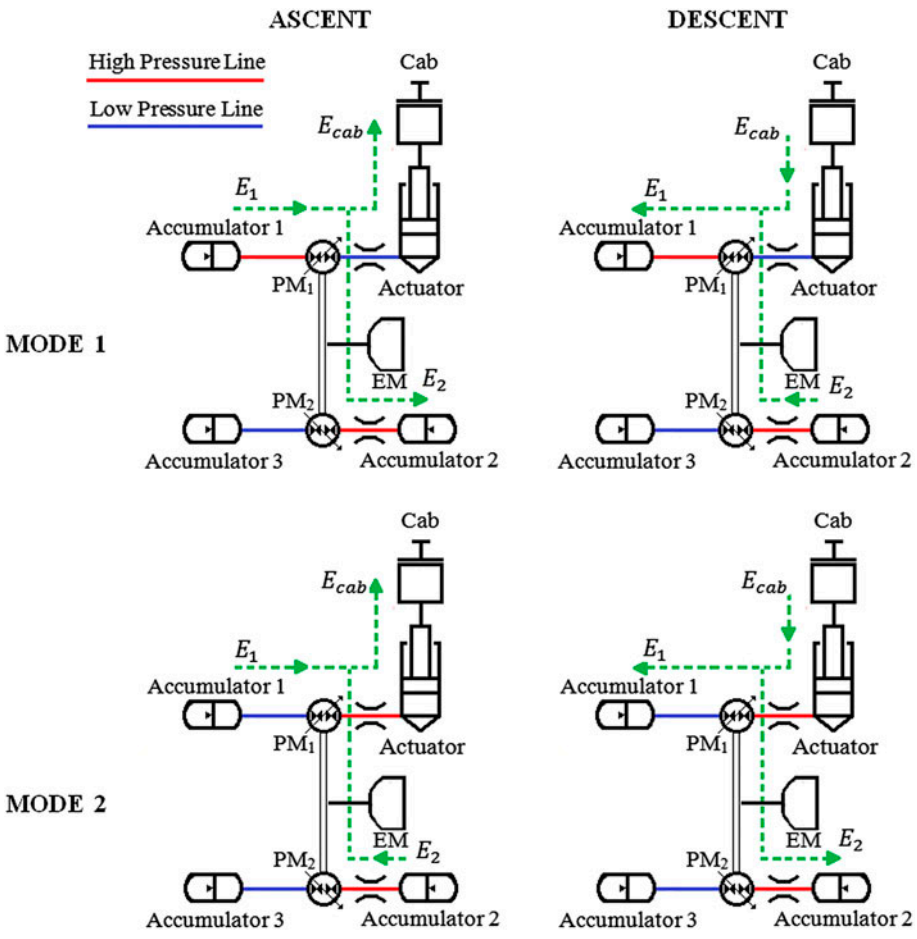

Figure A2. Energy flow through each operating mode during ascent and descent.

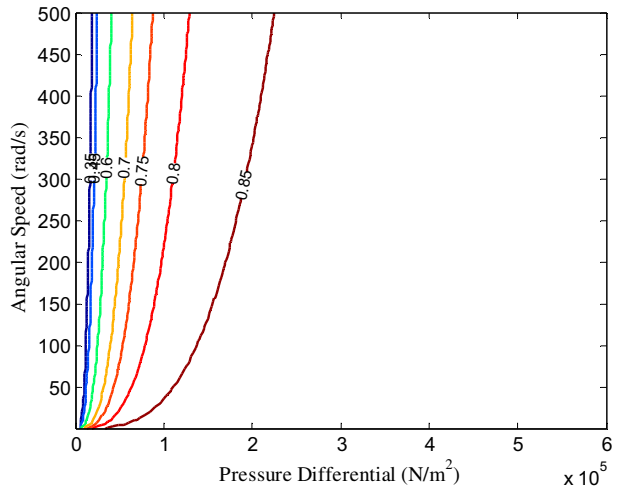

Figure A3. PM efficiency contours; constant displacement.

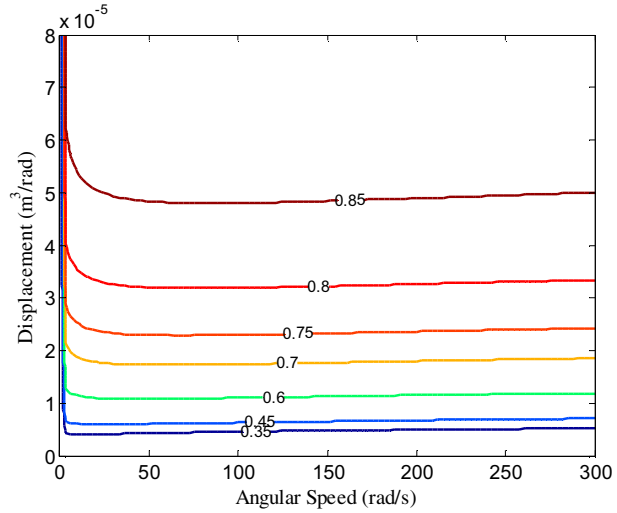

Figure A4. PM efficiency contours; constant differential pressure.

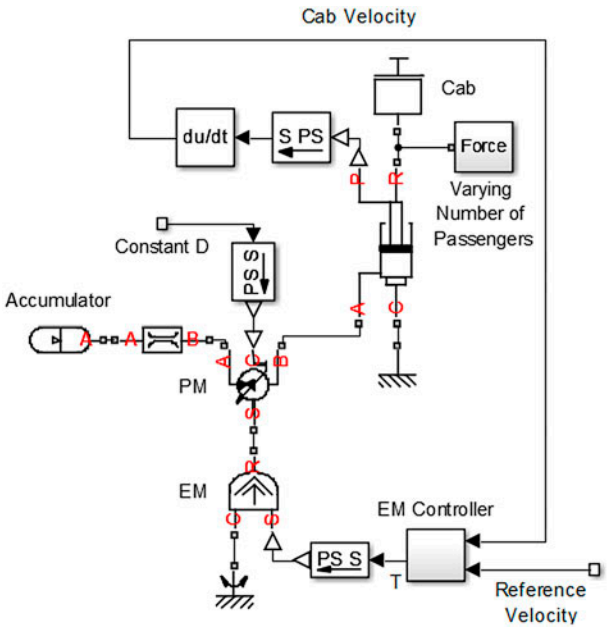

Figure A5. Simulink/SimScape model of the electrohydraulic system.

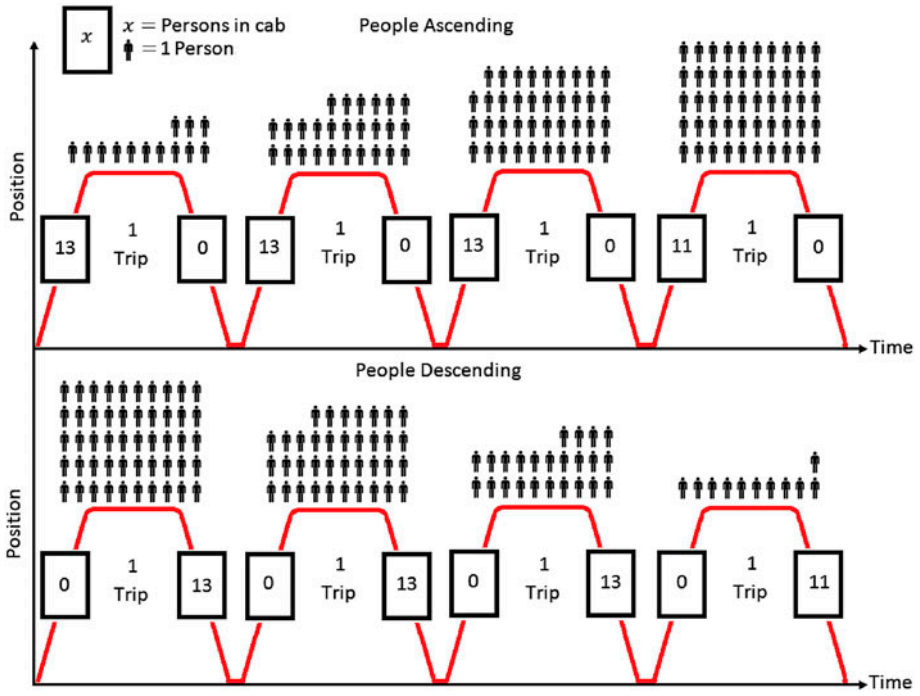

Figure A6. Full day operation for a cab load of 13 people for one floor; 8 trips per floor, for 3 floors (2nd, 3rd, and 4th) yields 24 trips total and 150 people moved.

Table A1. Parameters used for the SimScape model of the hydraulic architecture.

	Cab		
Mass (kg)	1100–2080		
	Cylinder		
Area (m^2)	0.0036		
Stroke (m)	20		
	Accumulator 1	*Accumulator 2*	*Accumulator 3*
Capacity (m^3)	0.15	0.14	0.11
Preload pressure (Pa)	9.25E+05	1.03E+07	6.90E+05
Initial volume (m^3)	0.087	0.021	0
	PM_1	*PM_2*	
Displacement (m^3/rad)	4.23E-05	1.15E-05	
	Hydraulic resistance 1	*Hydraulic resistance 2*	
Area (m^2)	0.006	0.006	
Flow discharge coeff.	0.7	0.7	
	PM_1 controller	*PM_2 controller*	
P gain (s-m^2/rad)	−4E-5	4E-5	
I gain (m^2/rad)	−9E-5	9E-5	
	EM controller		
P gain (N-s)	−0.01		
I gain (N)	0		
Reference pressure (Pa)	1.32E7		
	Motion		
Distance per floor (m)	3.65		
Max. velocity (m/s)	0.63		
Max. acceleration (m/s^2)	0.75		

Table A2. Parameters used for the SimScape model of the electrohydraulic system.

Cab	
Mass (kg)	1100–2080
Cylinder	
Area (m^2)	0.0036
Stroke (m)	20
Accumulator	
Capacity (m^3)	0.15
Preload pressure (Pa)	9.25E+05
Initial volume (m^3)	0.087
PM	
Displacement (m^3/rad)	4.23E-05
Hydraulic resistance	
Area (m^2)	0.006
Flow discharge coeff.	0.7
EM controller	
P gain (N-s)	500
I gain (N)	100

Table A3. Number of trips for a full day operation at each cab load.

Cab load (persons)	1	2	3	4	5	6	7	8	9	10	11	12	13	14
Trips	300	150	102	78	60	54	48	42	36	30	30	30	24	24